Dual-stimuli *in-situ* TEM study on the nonergodic/ergodic crossover in the $0.75(Bi_{1/2}Na_{1/2})TiO_3–0.25SrTiO_3$ relaxor

Zhongming Fan, and Xiaoli Tan[a)]

Department of Materials Science and Engineering, Iowa State University, Ames, IA 50011, USA

The existence of a variety of phases and their transitions in the electric field-temperature (E-T) space of relaxor ferroelectrics makes it an interesting research subject. To directly observe the evolution of domain morphology and crystal symmetry in ferroelectrics under either temperature change or an applied electric field, *in-situ* transmission electron microscopy (TEM) is often the preferred characterization technique. Accessing all the phases in the E-T space of a relaxor crystal requires *in-situ* TEM with capabilities of simultaneous heating and biasing. In this Letter, such a dual-stimuli *in-situ* TEM technique is demonstrated on $0.75(Bi_{1/2}Na_{1/2})TiO_3–0.25SrTiO_3$, a relaxor ceramic with a thermal depolarization temperature T_d of about 40 ºC. Not only the domain structure change during thermal depolarization is directly seen, but also different microstructural responses under an applied electric field in the nonergodic and ergodic states are observed. The results prove that the dual-stimuli *in-situ* TEM technique is indispensable to explore the rich physics in functional materials.

[a)]Author to whom correspondence should be addressed. Electronic mail: xtan@iastate.edu

In-situ transmission electron microscopy (TEM) is a powerful tool for nanoscale investigations on the materials behavior under external stimuli, such as mechanical stress, magnetic field, temperature change, and electric field.[1-4] In the field of ferroelectricity, heating/cooling *in-situ* TEM has been widely employed to study the temperature-dependent polar structures.[5,6] In order to explore the domain switching dynamics, electric field is, with no doubt, the most commonly introduced stimulus,[7-9] although mechanical stress was also applied occasionally.[10] Nevertheless, applying multiple stimuli simultaneously during *in-situ* TEM experiments has great advantages over single stimulus for elucidating complex physics issues in advanced materials,[11] of which a good example is the complex phase transitions in relaxor ferroelectrics.[12,13]

Unlike normal ferroelectrics with typically micron-sized domains, relaxor ferroelectrics are featured with nanodomains. Subjected to a critical poling field at certain temperatures, a relaxor to ferroelectric phase transition could take place, evidenced by the formation of large domains. The stability of the induced ferroelectric phase is dictated by the temperature.[14] Below the depolarization temperature (T_d), the relaxor phase is in nonergodic state and the induced ferroelectric phase (hence large domains) remains upon the removal of the poling field. On the contrary, at temperatures above T_d, the relaxor is in the ergodic state and the formed large ferroelectric domains disrupt into nanodomains during unloading of the applied field.[15] Many properties, such as ferroelectric fatigue resistance, can drastically change at the nonergodic/ergodic crossover.[16] To access the ferroelectric phase, the ergodic and nonergodic relaxor phases in the electric field-temperature (E-T) space and to directly visualize the domain structure change during transitions between these phases, *in-situ* TEM with simultaneous heating/cooling and electric biasing is required. We have previously demonstrated the field

cooling *in-situ* TEM technique and revealed the nonergodic/ergodic crossover in a $Pb(Mg_{1/3}Nb_{2/3})O_3$-based relaxor ferroelectric ceramic.[17] However, neither simultaneous biasing and heating *in-situ* TEM experiments nor a direct comparison of transitions of the nonergodic and the ergodic to the ferroelectric phase are reported in the literature. In the present work, dual-stimuli *in-situ* TEM tests are conducted on a $(Bi_{1/2}Na_{1/2})TiO_3$-based lead-free relaxor and distinct behaviors in nonergodic and ergodic regimes are directly observed.

The $0.75(Bi_{1/2}Na_{1/2})TiO_3$–$0.25SrTiO_3$ (BNST25) ceramic was fabricated using the solid-state reaction method, with starting powders of Bi_2O_3 (99.9%), Na_2CO_3 (99.9%), $SrCO_3$ (99.99%) and TiO_2 (99.99%). The batched powder was mixed in a vibratory mill in ethanol for 6 hours, and then dried in oven at 90°C. Calcination was performed at 850 °C for 2 hours while sintering was carried out at 1100 °C for 2 hours. The temperature-dependent dielectric constant and loss tangent were measured at a heating rate of 4 ºC/min using an LCZ meter (3330; Keithley, Cleveland, OH). The polarization hysteresis and electro-strain were recorded at 1 Hz using a standardized ferroelectric test system (Precision LC II, Radiant Technologies) and MTI-2000 Fotonic Sensor (MTI Instruments Inc), respectively. For the *in-situ* TEM experiments on a FEI Tecnai G2-F20 microscope, as-sintered pellets were mechanically ground and polished to 120 μm thickness. Disks of 3 mm in diameter were ultrasonically cut and the center portion was thinned to 10 μm by mechanical dimpling. The dimpled disks were annealed at 250 ºC for 1 hour to minimize the residual stress before Ar-ion milling until perforation. Two types of *in-situ* TEM experiments were performed. The single stimulus *in-situ* heating TEM tests were conducted with a double-tilt specimen holder while the dual-stimuli *in-situ* heating+biasing TEM tests were carried out with on a custom-made single-tilt holder.

The temperature dependence of the microstructure in unpoled BNST25 is first investigated using the single stimulus *in-situ* heating specimen holder. Figure 1 shows a grain observed along the $[11\bar{2}]_c$ zone-axis. At 25 ºC, the grain is occupied with nanodomains (Fig. 1a), which is similar to other BNT-based relaxors with compositions close to the morphotropic phase boundary.[18,19] Upon heating, the initial domain morphology remains almost unchanged until ~200 ºC when the grain becomes contrast-free (Fig. 1b). In addition, the evolution of the selected area electron diffraction pattern is monitored during the *in-situ* heating. At 25 ºC, discrete ½{*ooo*} type superlattice diffraction spots are clearly seen (highlighted with the bright circle in Fig. 1c$_1$). Around 50 ºC, another set of superlattice spots, ½{*ooe*} type marked with the bright arrow, appears (Fig. 1c$_2$). It is noted that the ½{*ooe*} spots are considerably weaker than the ½{*ooo*} spots. As temperature continues increasing, the ½{*ooo*} spots gradually become diffuse while the ½{*ooe*} spots exhibit no apparent intensification (Fig. 1c$_3$). At 200 ºC, both sets of superlattice spots are hardly detectable (Fig. 1c$_4$). The electron diffraction results suggest that two phase transitions take place during heating of BNST25 from room temperature to 200 ºC. Since the ½{*ooo*} and ½{*ooe*} superlattice spots are considered signatures of the rhombohedral *R3c* and the tetragonal *P4bm* phases, respectively, in BNT-based perovskite ceramics,[18,20] their temperature evolution indicates that a small fraction of the nanodomains transform from rhombohedral to tetragonal below 50 ºC and most of the nanodomains disappear when the symmetry becomes cubic around 200 ºC.

Despite that the rhombohedral-tetragonal phase transition is believed to reflect the nonergodic to ergodic transition,[6] the crossover cannot be convincingly visualized in bright-field micrographs. This calls for the heating+biasing *in-situ* TEM capability. Using the dual-stimuli specimen holder, another grain is examined with the electron beam close to its $[001]_c$ zone-axis

(Fig. 2). First, at room temperature subjected to the poling field, wedge-shaped large domains are observed to develop out of the initial nanodomains (Figs. 2a, 2b). Moreover, the long domain walls trace along the $<100>_c$ direction (Fig. 2b), suggesting that they are very likely inclined $\{110\}_c$ planes. Then the applied field is removed and the specimen is heated. Within a very narrow temperature window (from 25 to 46 ºC), the large domains vanish and the entire grain is full of nanodomains again (Fig. 2c). Apparently this is the thermal depolarization process of the poled BNST25 ceramic. The abrupt depolarization process revealed by the dual-stimuli *in-situ* TEM is corroborated by the dielectric measurement on a bulk ceramic sample (Fig. 3). In a poled BNST25 ceramic, the dielectric constant shows obvious frequency dispersion below $T_m \approx 190$ ºC (Fig. 3a). Apart from this dividing point between relaxor and paraelectric regimes,[15] no apparent anomalies are present in the dielectric constant curve. On the other hand, the loss tangent curve reveals another local maximum point at ~40 ºC (Fig. 3b). In contrast, the loss tangent curve from an annealed sample is much smoother (inset of Fig. 3b).[21] This is in good consistence with the fact that the thermal depolarization process is found to be much more significant in a poled grain (Fig. 2) than an unpoled one (Fig. 1).

To further discern the microstructural responses to the poling field in the nonergodic and ergodic state of BNST25, another *in-situ* heating+biasing TEM test is carried out (Fig. 4). The grain of interest is initially full of nanodomains (Fig. 4a). Due to the limitation of the single-tilt specimen holder, the grain is not aligned to a special zone-axis. When a voltage of 360 V is applied to the ceramic at 25 ºC, wedge-shaped large ferroelectric domains form (Fig. 4b). Note that the vertical feature that intersects with the large domains is not likely a field-induced domain. It is more likely a pre-existing dislocation or planar defect whose contrast is sensitive to the specimen tilt; it becomes invisible in Fig. 4e and 4f under slightly different tilting conditions.

After the voltage is removed, the large domains preserve while some domains seem to grow wider (Fig. 4c). The induced ferroelectric phase is, hence, metastable and the nonergodic state of the ceramic is verified. The specimen is then heated until the majority of large domains depolarize around 41 °C (Fig. 4d). Keeping the temperature for two minutes, electric bias is re-applied. It is found that large ferroelectric domains won't develop again until a higher voltage (420 V) is reached (Fig. 4e). Interestingly, these large domains are no longer in wedge shape but take a lamellar morphology with dense straight domain walls. More importantly, nanodomains are recovered upon removal of the applied voltage (Fig. 4f). Such a reversible relaxor ↔ ferroelectric transition confirms the ergodic nature of BNST25 at the test temperature (41 °C).

Our dual-stimuli *in-situ* TEM results clearly reveal the nonergodic/ergodic crossover and their different behaviors during the transition to the ferroelectric phase. To correlate the microstructural responses with macroscopic properties, electrical tests are also conducted on a bulk ceramic (Fig. 5). At room temperature, BNST25 displays the typical square polarization vs electric field (P-E) loop and the butterfly-shaped strain-field (S-E) loop. At 50 °C, the P-E loop becomes pinched while the S-E loop changes to sprout shape with a peak strain of ~0.3%.[22] Below T_d, BNST25 is in nonergodic relaxor phase and the nanodomains have a rhombohedral *R3c* symmetry (Fig. 1c$_1$).[23] Under the poling field, the nanodomains transform to wedge-shaped large domains that is the typical shape for rhombohedral perovskite (Figs. 2b and 4c).[24] In other words, the relaxor to ferroelectric phase transition does not lead to the change in crystal symmetry. This is quite similar to the situation in $Pb(Mg_{1/3}Nb_{2/3})O_3$ where both the relaxor and ferroelectric phases take the same *R3m* structure.[15] Due to the nonergodicity, BNST25 preserves the induced ferroelectric phase and gives rise to the ferroelectric-like polarization or strain loop. Above T_d, BNST25 contains a mixture of major *R3c* and minor *P4bm* phases (Fig. 1c$_2$). Complex

phase transitions may occur under a poling field. As with our previous work on $(Bi_{1/2}Na_{1/2})TiO_3$–$BaTiO_3$ ceramics,[18] the minor *P4bm* phase could be transformed to the *R3c* phase during the electrical poling process. On the other hand, deduced from the unique morphology of long and thin domains (Fig. 4e), these thin lamellar domains could result from coalescence of the *P4bm* nanodomains during the relaxor to ferroelectric phase transition.[25] Since electron diffraction analysis is not feasible for this grain using the single-tilt holder, the possibility of a transition to the *P4mm* tetragonal symmetry cannot be ruled out.[26] Due to the ergodicity at temperatures above T_d, the lamellar domains disrupt into nanodomains once the field is unloaded, resulting in the pinched P-E loop with reduced remanent polarization and the sprout-shaped S-E loop with almost zero remanent strain.

Additionally, a close examination of Fig. 5 can reveal interesting subtle contrasts between the nonergodic and the ergodic phases. As shown in Fig. 5a, even though the remanent polarization is considerably suppressed, the maximum polarization is slightly higher (~4.5%) in the ergodic phase.[27] This contrast might be correlated with whether the dipole alignment is realized through phase transition or domain coalescence. In Fig. 5b, the critical field is quantified as 16.2 kV/cm at 25 ºC while it is 18.8 kV/cm at 50 ºC. The rate of increase here is roughly the same as the increase in the applied bias in the TEM test (Fig. 4, a 16% increase from 360 V to 420 V). Therefore, the change in the reversibility at the nonergodic/ergodic crossover in BNST25 may reflect the change in the phase transitions mechanisms.

In summary, the dual-stimuli *in-situ* TEM technique with simultaneous heating and biasing capabilities is demonstrated to access different phases and their transitions in the E-T space of a lead-free ceramic. In the nonergodic state of BNST25, the nanodomains are observed to coalesce into large ferroelectric domains during poling which are preserved after the field is removed. In

the ergodic state, complicated phase transitions are likely to take place during field loading and reverse transitions occur during unloading to resume the initial microstructure. Correspondingly, a large remanent polarization and a butterfly-shaped strain loop are recorded on macroscopic properties of the nonergodic state; and a suppressed remanent polarization and an almost zero remanent strain are seen in the ergodic state.

This work was supported by the National Science Foundation (NSF) through Grant DMR-1465254.

[1] Z. W. Shan, R. K. Mishra, S. A. Syed Asif, O. L. Warren, and A. M. Minor, Nat. Mater. **7**, 115 (2008).

[2] L. Zhou, E. White, L. Ke, D. A. Cullen, P. Lu, S. Constantinides, R. W. McCallum, I. E. Anderson, and M. J. Kramer, J. Magn. Magn. Mater. **471**, 142 (2019).

[3] T. Ma, S. Wang, M. Chen, R. Maligal-Ganesh, L. -L. Wang, D. D. Johnson, M. J. Kramer, W. Huang, and L. Zhou, Chem. **5**, (2019).

[4] J. Y. Huang, L. Zhong, C. M. Wang, J. P. Sullivan, W. Xu, L. Q. Zhang, S. X. Mao, N. S. Hudak, X. H. Liu, A. Subramanian, H. Fan, L. Qi, A. Kushima, and J. Li, Science **330**, 1515 (2010).

[5] D. Viehland, Phys. Rev. B **52**, 778 (1995).

[6] Z. Fan, L. Zhou, T. -K. Kim, J. Zhang, S. -T. Zhang, and X. Tan, Phys. Rev. Mater. **3**, 024402, (2019).

[7] Z. Fan, C. Zhou, X. Ren, and X. Tan, Appl. Phys. Lett. **111**, 252902 (2017).

[8] Y. Sato, T. Hirayama, and Y. Ikuhara, Appl. Phys. Lett. **100**, 172902 (2012).

[9] C. T. Nelson, P. Gao, J. R. Jokisaari, C. Heikes, C. Adamo, A. Melville, S. -H. Baek, C. M. Folkman, B. Winchester, Y. Gu, Y. Liu, K. Zhang, E. Wang, J. Li, L. -Q. Chen, C. -B. Eom, D. G. Schlom, and X. Pan, Science **334**, 968 (2011).

[10] P. Gao, J. Britson, C. T. Nelson, J. R. Jokisaari, C. Duan, M. Trassin, S. -H. Baek, H. Guo, L. Li, Y. Wang, Y. -H. Chu, A. M. Minor, C. -B. Eom, R. Ramesh, L. -Q. Chen, and X. Pan, Nat. Commun. **5**, 3801 (2014).

[11] F. Börrnert, H. Müller, T. Riedel, M. Linck, A. I. Kirkland, M. Haider, B. Büchner, and H. Lichte, Ultramicroscopy **151**, 31 (2015).

[12] K. Aizu, Rev. Mod. Phys. **34**, 550 (1962).

[13] K. Aizu, Phys. Rev. B **2**, 754 (1970).

[14] C. J. Stringer, and C. A. Randall, J. Am. Ceram. Soc. **90**, 1802 (2007).

[15] A. A. Bokov and Z. -G. Ye, J. Mater. Sci. **41**, 31 (2006).

[16] Z. Luo, T. Granzow, J. Glaum, W. Jo, J. Rödel, M. Hoffman, J. Am. Ceram. Soc. **94**, 3927 (2011).

[17] W. Qu, X. Zhao, and X. Tan, Appl. Phys. Lett. **89**, 022904 (2006).

[18] C. Ma, H. Guo, S. P. Beckman, and X. Tan, Phys. Rev. Lett. **109**, 107602 (2012).

[19] Z. Fan, X. Liu, and X. Tan, J. Am. Ceram. Soc. **100**, 2088 (2017).

[20] D. I. Woodward and I. M. Reaney, Acta Cryst. B **61**, 387 (2005).

[21] W. Jo, S. Schaab, E. Sapper, L. A. Schmitt, H. -J. Kleebe, A. J. Bell, and J. Rödel, J. Appl. Phys. **110**, 074106 (2011).

[22] Y. Hiruma, Y. Imai, Y. Watanabe, H. Nagata, and T. Takenaka, Appl. Phys. Lett. **92**, 262904 (2008).

[23] J. -H. Cho, J. -S. Park, S. -W. Kim, Y. -H. Jeong, J. -S. Yun, W. -I. Park, Y. -W. Hong, and J. -H. Park, J. Eur. Ceram. Soc. **37**, 3313 (2017).

[24] J. Ricote, R. W. Whatmore, and D. J. Barber, J. Phys. Condens. Matter **12**, (2000) 323.

[25] H. Guo, C. Ma, X. Liu, and X. Tan, Appl. Phys. Lett. **102**, 092902 (2013).

[26] S. Kim, H. Choi, S. Han, J. S. Park, M. H. Lee, T. K. Song, M. -H. Kim, D. Do, and W. -J. Kim, J. Eur Ceram. Soc. **37**, 1379 (2017).

[27] E. Sapper, N. Novak, W. Jo, T. Granzow, and J. Rödel, J. Appl. Phys. **115**, 194104 (2014).

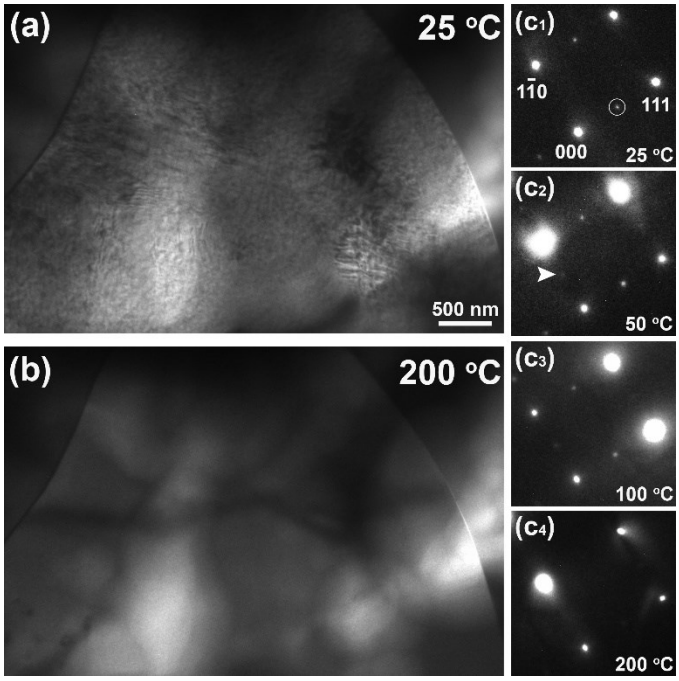

Fig.1. Bright field micrographs of a representative grain in BNST25 along the $[11\bar{2}]_c$ zone axis at (a) 25 and (b) 200 °C. (c_1)-(c_4) Selected area electron diffraction patterns recorded at 25, 50, 100, and 200 °C.

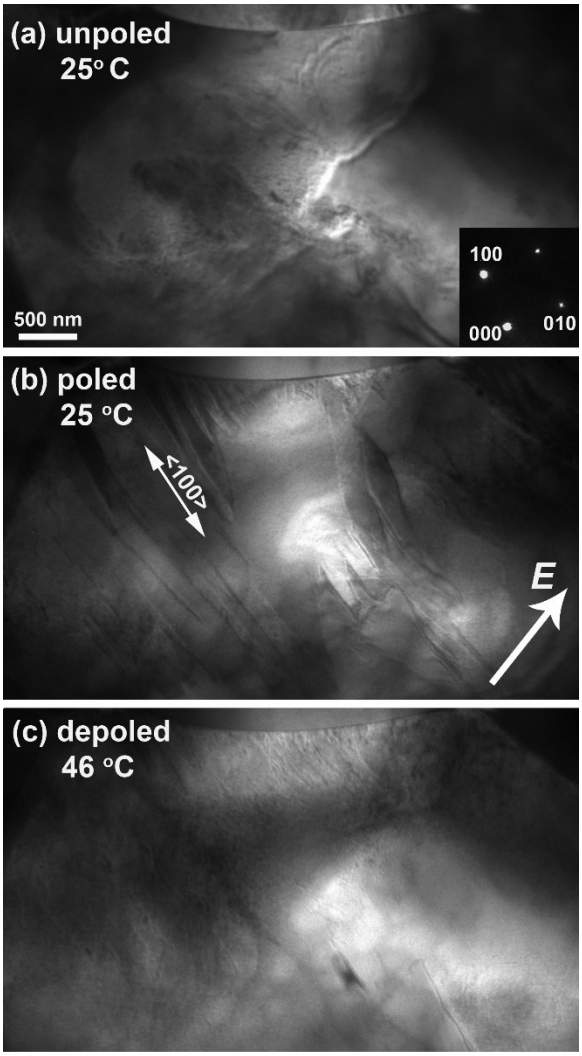

Fig. 2. Dual-stimuli *in-situ* TEM on the domain morphology in a grain aligned close to the $[001]_c$ zone-axis in the (a) unpoled, (b) poled, and (c) depoled state. The bright arrow in (b) indicates the direction of the poling field.

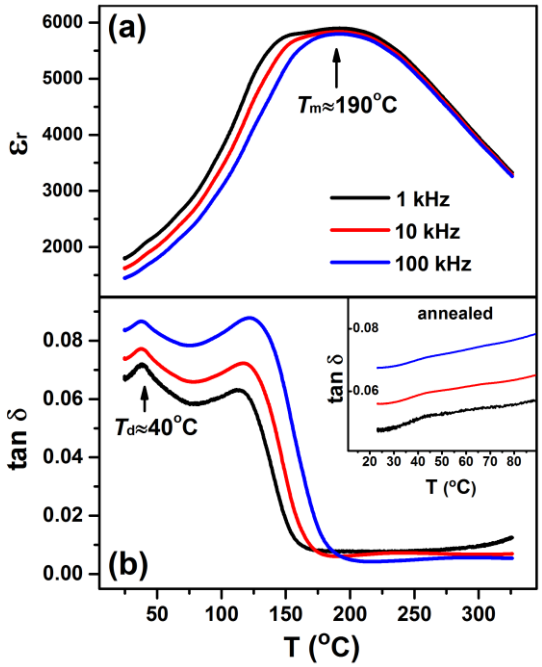

Fig. 3. (a) Dielectric constant (ε_r), and (b) loss tangent (tan δ) as a function of temperature measured in a poled bulk ceramic. The inset in (b) shows the loss tangent curve obtained from the annealed sample.

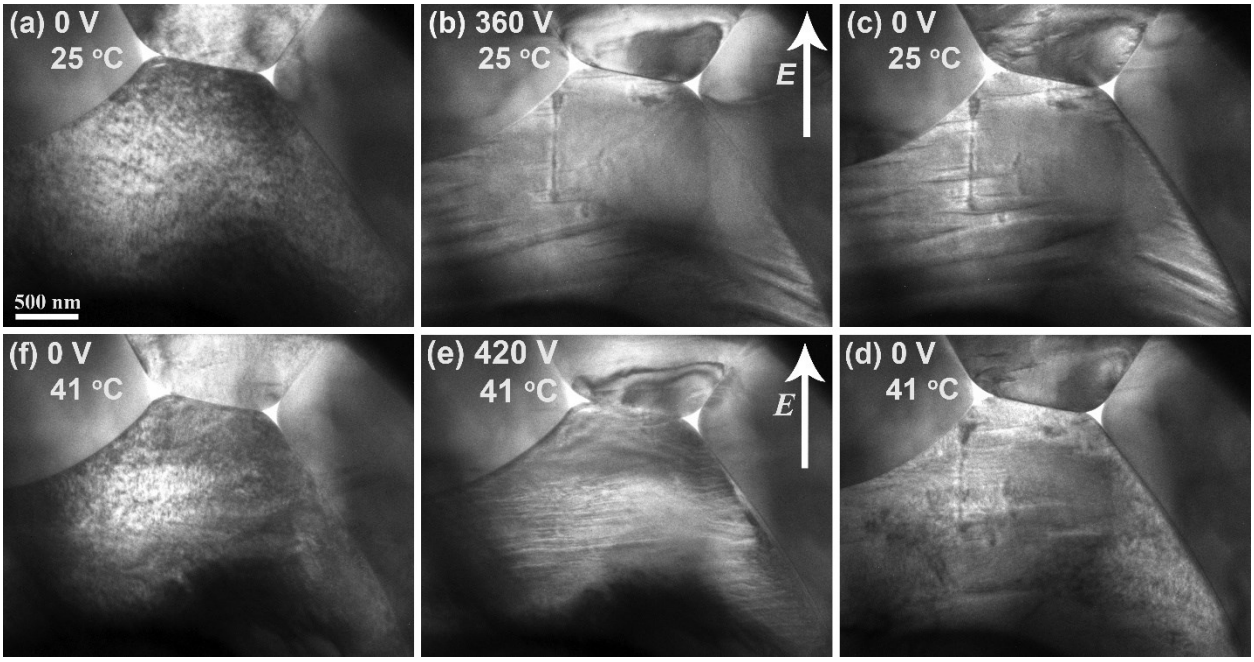

Fig. 4. Dual-stimuli *in-situ* TEM on another BNST25 specimen. The bright field micrographs of a grain at (a) 0 V, 25 °C; (b) 360 V, 25 °C; (c) 0 V, 25 °C; (d) 0 V, 41 °C; (e) 420 V, 41 °C; (f) 0 V, 41 °C. This is also the experiment sequence. The bright arrows in (b) and (e) represents the direction of the applied field.

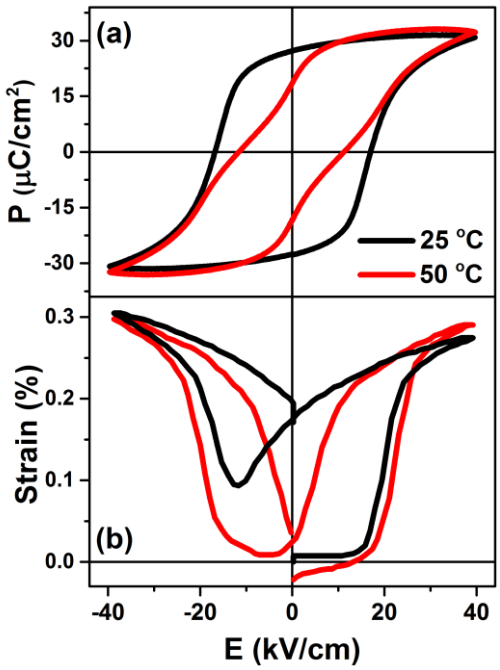

Fig. 5. The (a) P-E and (b) S-E hysteresis loop measured in a bulk ceramic sample at 1 Hz at 25 and 50 °C.